

Constrained Policy Gradient Method for Safe and Fast Reinforcement Learning: a Neural Tangent Kernel Based Approach

Balázs Varga^{1*}, Balázs Kulcsár¹ and Morteza Haghir Chehreghani²

^{1*}Department of Electrical Engineering, Chalmers University of Technology, Hörsalsvägen 11, Gothenburg, Sweden.

²Department of Computer Science and Engineering, Chalmers University of Technology, Hörsalsvägen 11, Gothenburg, Sweden.

Contributing authors: balazsv@chalmers.se; kulcsar@chalmers.se; morteza.chehreghani@chalmers.se;

Abstract

This paper presents a constrained policy gradient algorithm. We introduce constraints for safe learning with the following steps. First, learning is slowed down (lazy learning) so that the episodic policy change can be computed with the help of the policy gradient theorem and the neural tangent kernel. Then, this enables us the evaluation of the policy at arbitrary states too. In the same spirit, learning can be guided, ensuring safety via augmenting episode batches with states where the desired action probabilities are prescribed. Finally, exogenous discounted sum of future rewards (returns) can be computed at these specific state-action pairs such that the policy network satisfies constraints. Computing the returns is based on solving a system of linear equations (equality constraints) or a constrained quadratic program (inequality constraints, regional constraints). Simulation results suggest that adding constraints (external information) to the learning can improve learning in terms of speed and transparency reasonably if constraints are appropriately selected. The efficiency of the constrained learning was demonstrated with a shallow and wide ReLU network in the Cartpole and Lunar Lander OpenAI gym environments. The main novelty of the paper is giving a practical use of the neural tangent kernel in reinforcement learning.

1 Introduction

In reinforcement learning (RL), the agent learns in a trial and error way. In a real setting, it can lead to undesirable situations which may result in damage or injury of the agent or the environment system. In addition, the agent might waste a significant amount of time exploring irrelevant regions of the state and action spaces. Safe RL can be defined as the process of learning policies that maximize the expectation of the return in problems under safety constraints. Thus, safe exploration often includes some prior knowledge of the environment (e.g., a model Berkenkamp et al. (2017); Fisac et al. (2018); Zimmer et al. (2018)) or has a risk metric Garcia and Fernandez (2015); Turchetta et al. (2020). In RL, safety can be guaranteed in a probabilistic way. Learning in this context aims to strike a balance between exploration and exploitation so that the system remains within a safe set. On the other hand, in a safety-critical setting, exploration cannot be done blindly. Therefore, some sort of knowledge of the environment is vital.

Constrained learning is an intensively studied topic, having close ties to safe learning Yang (2019). Han et al. (2008) argues that constrained learning has better generalization performance and a faster convergence rate. Tessler et al. (2018) presents a constrained policy optimization, which uses an alternative penalty signal to guide the policy. Uchibe and Doya (2007) proposes an actor-critic method with constraints that define the feasible policy space.

In policy gradient methods, the function approximator predicts action values or probabilities from which the policy can be derived directly. Finding the parameters of the agent is done via optimization (gradient ascent) following the policy gradient theorem Sutton and Barto (2018). Policy gradient methods have many variants and extensions to improve their learning performance Zhang et al. (2021). For example, in Kakade (2001) a covariant gradient is defined based on the underlying structure of the policy. Whiteson (2020) deduced expected policy gradients for actor-critic methods. Cheng et al. (2020) deals with the reduction of the variance in Monte-Carlo (MC) policy gradient methods.

In this work we use priori knowledge of the environment not to build a model, rather than to impose some constraints on the policy. We develop a deterministic policy gradient algorithm (based on REINFORCE, Williams (1987)) augmented with different types of constraints via shaping the rewards. Opposed to Altman et al. (2019), transition probabilities are not explicitly replaced with taboo states but constraints are imposed on these transition probabilities via solving a constrained quadratic program. Therefore, compared to Tessler et al. (2018), training does not rely on non-convex optimization or additional heuristics. Safety in our approach is guaranteed by the careful selection of constraints and the success of the optimization.

The key ingredient in our work is the Neural Tangent Kernel (NTK, Jacot et al. (2018)). "It the evolution of fully connected neural networks under gradient descent in function space. Dual to this perspective is an understanding of how neural networks evolve in parameter space, since the NTK is defined in

terms of the gradient of the NN’s outputs with respect to its parameters. In the infinite width limit, the connection between these two perspectives becomes especially interesting. The NTK remaining constant throughout training at large widths co-occurs with the NN being well described throughout training by its first order Taylor expansion around its parameters at initialization” Sohl-Dickstein et al. (2020). In this work, we exploit the NTK to compute the future policy using the above properties (fully connected, very wide NN, slow learning rate).

Earlier, policy iteration has been used in conjunction with NTK for learning the value function Goumiri et al. (2020). On the other hand, it was used in its analytical form as the covariance kernel of a GP (Novak et al. (2019); Rasmussen et al. (2003); Yang and Salman (2019)). Here, we directly use the NTK to project a one-step policy change in conjunction with the policy gradient theorem. Then, safety is incorporated via constraints. It is assumed that there are states where the agent’s desired behaviour is known. At these ”safe” states action probabilities are prescribed as constraints for the policy. Finally, returns are computed in such a way that the agent satisfies the constraints. This assumption is mild when considering physical systems: limits of a controlled system (saturation) or desired behavior at certain states are usually known (i.e., the environment is considered a gray-box). The proposed algorithm is developed for continuous state spaces and discrete action spaces. According to the proposed categorization in Garcia and Fernandez (2015), the proposed algorithm falls into constrained optimization with external knowledge.

The contribution of the paper is twofold. First, we analytically give the policy evolution under gradient flow, using the NTK. Second, we extend the REINFORCE algorithm with constraints. Our variant of the REINFORCE algorithm converges within a few episodes if constraints are set up correctly. The constrained extension relies on computing extra returns via convex optimization. In conclusion, the paper provides a practical use of the neural tangent kernel in reinforcement learning.

The paper is organized as follows. First, we present the episode-by-episode policy change of the REINFORCE algorithm (Section 2.1). Then, relying on the NTK, we deduce the policy change at unvisited states, see Section 2.2. Using the results in Section 2.2, we compute returns at arbitrary states in Section 3. We introduce equality constraints for the policy by computing ”safe” returns by solving a system of linear equations (Section 3.1). In the same context, we can enforce inequality constraints by solving a constrained quadratic program, see Section 3.2. Additionally, we explore various ways to enforce constraints on a whole region (Section 3.3). In Section 4.1 we investigate the proposed learning algorithm in two OpenAI gym environments: in the Cartpole environment and in the Lunar Lander (Section 4.2). Finally, we summarize the findings of this paper in Section 5.

2 Kernel-based analysis of the REINFORCE algorithm

In this section, the episode-by-episode learning dynamics of a policy network is analyzed and controlled in a constrained way. To this end, first we introduce the RL framework and the REINFORCE algorithm. Then, the learning dynamics of a wide and shallow neural network is analytically given. Finally, returns are calculated that force the policy to obey equality and inequality constraints at specific states.

2.1 Reformulating the learning dynamics of the REINFORCE algorithm

Reinforcement learning problems are commonly introduced in a Markov Decision Process (MDP) setting Sutton and Barto (2018). Similarly, the most common way of tackling safe RL is through constrained MDPs. I.e., safety is ensured via constraining the MDP: at given states some actions that are deemed unsafe are forbidden Altman (1999); Wachi and Sui (2020).

Let the 5-tuple $(\mathcal{S}, \mathcal{A}, \underline{P}, \mathcal{R}(s), \gamma)$ characterize an MDP. This tuple consists of the continuous state space with n_n dimensions $\mathcal{S} \subseteq \mathbb{R}^{n_n}$, the discrete action space $\mathcal{A} \subset \mathbb{Z}^{n_a}$, the transition probability matrix \underline{P} , the reward function $\mathcal{R}(s) \in \mathbb{R}$, and the discount factor $\gamma \in]0, 1]$. The agent traverses the MDP following the policy $\pi(a | s, \theta)$.

In the reinforcement learning setup, the goal is maximizing the (discounted sum of future) rewards in episode e

$$J(\theta) = \mathbb{E}_\pi(G_e). \quad (1)$$

Then, policy gradient methods learn by applying the policy gradient theorem.

Theorem 1 *Policy Gradient Theorem. Sutton and Barto (2018)* *The derivative of the expected reward is the expectation of the product of the reward and gradient of the log of the policy*

$$\frac{\partial}{\partial \theta} \mathbb{E}_\pi(G_e) = \mathbb{E}_\pi \left(G_e \frac{\partial}{\partial \theta} \log \pi(a | s, \theta) \right). \quad (2)$$

Learning means tuning the weights of a function approximator (agent) episode-by-episode. In most cases the function approximator is a Neural Network Arulkumaran et al. (2017); Silver et al. (2014). If the training is successful, then the function approximator predicts values or probabilities from which the policy can be derived. More specifically, the output of the policy gradient algorithm is a probability distribution, which is characterized by the function approximator's weights.

In this paper we deal with the a simple policy gradient methods called the REINFORCE algorithm Williams (1987); Szepesvári (2010). In REINFORCE, the agent learns the policy directly by updating its weights $\theta(e)$ using Monte-Carlo episode samples. Thus, the expectation in Eq. (2) turns into summation. One realization is generated with the current policy (at episode e) $\pi(a_e | s_e, \theta(e))$. Assuming continuous state space, and discrete action space the episode batch (with length n_B) is $\{\underline{s}_e(k), \underline{a}_e(k), r_e(k)\}$, for all $k = 1, 2, \dots, n_B$, where $\underline{s}_e(k) \in \mathcal{S}$ is the n_n dimensional state vector in the k^{th} step of the MC trajectory, $\underline{a}_e(k) \in \mathcal{A}$ is the action taken, and $r_e(k) \in \mathcal{R}(s)$ is the reward in step k . For convenience, the states, actions, and rewards in batch e are organized into columns $\underline{s}_e \in \mathbb{R}^{n_B \times n_n}$, $\underline{a}_e \in \mathbb{Z}^{n_B}$, $r_e \in \mathbb{R}^{n_B}$, respectively. The REINFORCE algorithm learns as summarized in Algorithm 1. The update rule is based on the policy gradient theorem Sutton and Barto (2018) and for the whole episode it can be written as the sum of gradients induced by the batch:

$$\theta(e+1) = \theta(e) + \alpha \sum_{k=1}^{n_B} \left(G_e(k) \frac{\partial}{\partial \theta} \log \pi(\underline{a}_e(k) | \underline{s}_e(k), \theta(e)) \right)^T \quad (3)$$

Algorithm 1 The REINFORCE algorithm

- 1: Initialize $e = 1$.
- 2: Initialize the policy network with random θ weights.
- 3: **while** not converged **do**
- 4: Generate a Monte-Carlo trajectory $\{\underline{s}_e(k), \underline{a}_e(k), r_e(k)\}$,
 $k = 1, 2, \dots, n_B$ with the current policy $\pi(\underline{a}_e(k) | \underline{s}_e(k), \theta(e))$.
- 5: **for** the whole MC trajectory ($k = 1, 2, \dots, n_B$) **do**
- 6: Estimate the return as

$$G_e(k) = \sum_{\kappa=k+1}^{n_B} \gamma^{\kappa-k} r_e(\kappa) \in \mathbb{R} \quad (4)$$

- 7: Update policy parameters with gradient ascent according to Eq. (3).
 - 8: **end for**
 - 9: Increment e .
 - 10: **end while**
-

Taking Algorithm 1 further, it is possible to compute the episodic policy change $\frac{\partial \pi(\underline{a}_e | \underline{s}_e, \theta(e))}{\partial e}$ with respect to every element in batch e , assuming gradient flow ($\alpha \rightarrow 0$). Note that $\underline{\pi}(\underline{a}_e | \underline{s}_e, \theta(e))$ is now vector-valued since we are dealing with the whole batch.

Theorem 2 Given batch $\{\underline{s}_e(k), \underline{a}_e(k), r_e(k)\}_{k=1}^{n_B}$, and assuming gradient flow, the episodic policy change with the REINFORCE algorithm at the batch state-action pairs

are

$$\frac{\partial \pi(\underline{a}_e | \underline{s}_e, \theta(e))}{\partial e} = \underline{\Theta}_{\pi, e}(s, s') \underline{\Pi}_e^I(\underline{s}_e, \underline{a}_e, \theta(e)) \underline{G}_e(\underline{r}_e),$$

where $\underline{\Theta}_{\pi, e}(s, s') \in \mathbb{R}^{n_B \times n_B}$ is the neural tangent kernel, $\underline{\Pi}_e^I(\underline{s}_e, \underline{a}_e, \theta(e)) \in \mathbb{R}^{n_B \times n_B}$ is a diagonal matrix containing the inverse policies (if they exist) at state-action pairs of batch e , and $\underline{G}_e(\underline{r}_e) \in \mathbb{R}^{n_B}$ is the vector of returns.

Proof Assuming very small learning rate α , the update algorithm (gradient ascent) can be written in continuous form (gradient flow) Parikh and Boyd (2014):

$$\frac{d\theta(e)}{de} = \sum_{k=1}^{n_B} \left(G_e(k) \frac{\partial}{\partial \theta} \log \pi(\underline{a}_e(k) | \underline{s}_e(k), \theta_e) \right)^T. \quad (5)$$

Furthermore, to avoid division by zero, it is assumed that the evaluated policy is strictly positive. The derivative on the left hand side is a column vector with size n_θ . Denote $\underline{s}_e = \{\underline{s}_e(k)\}_{k=1}^{n_B}$, $\underline{a}_e = \{\underline{a}_e(k)\}_{k=1}^{n_B}$, $\underline{r}_e = \{\underline{r}_e(k)\}_{k=1}^{n_B}$ and rewrite the differential equation in vector form as

$$\frac{d\theta(e)}{de} = \dot{\underline{\Pi}}_{\log}(\underline{s}_e, \underline{a}_e, \theta(e)) \underline{G}_e(\underline{r}_e), \quad (6)$$

where

$$\underline{G}_e(\underline{r}_e) = [G_e(1), G_e(2), \dots, G_e(n_B)]^T \quad (7)$$

is the vector of returns in episode e (Eq. (4)). The matrix of partial log policy derivatives ($\dot{\underline{\Pi}}_{\log}(\underline{s}_e, \underline{a}_e, \theta(e)) \in \mathbb{R}^{n_\theta \times n_B}$) is

$$\dot{\underline{\Pi}}_{\log}(\underline{s}_e, \underline{a}_e, \theta(e)) = \begin{bmatrix} \frac{\partial \log \pi(\underline{a}_e(1) | \underline{s}_e(1), \theta(e))}{\partial \theta_1} & \dots & \frac{\partial \log \pi(\underline{a}_e(n_B) | \underline{s}_e(n_B), \theta(e))}{\partial \theta_1} \\ \frac{\partial \log \pi(\underline{a}_e(1) | \underline{s}_e(1), \theta(e))}{\partial \theta_2} & \dots & \frac{\partial \log \pi(\underline{a}_e(n_B) | \underline{s}_e(n_B), \theta(e))}{\partial \theta_2} \\ \vdots & \ddots & \vdots \\ \frac{\partial \log \pi(\underline{a}_e(1) | \underline{s}_e(1), \theta(e))}{\partial \theta_{n_\theta}} & \dots & \frac{\partial \log \pi(\underline{a}_e(n_B) | \underline{s}_e(n_B), \theta(e))}{\partial \theta_{n_\theta}} \end{bmatrix}, \quad (8)$$

where subscripts of θ denote weights and biases of the policy network. By using an element-wise transformation $\frac{\log f(t)}{dx} = \frac{f'(t)}{f(t)}$, $\dot{\underline{\Pi}}_{\log}(\underline{s}_e, \underline{a}_e, \theta(e))$ can be rewritten as a product:

$$\dot{\underline{\Pi}}_{\log}(\underline{s}_e, \underline{a}_e, \theta(e)) = \begin{bmatrix} \frac{\partial \pi(\underline{a}_e(1) | \underline{s}_e(1), \theta(e))}{\partial \theta_1} & \dots & \frac{\partial \pi(\underline{a}_e(n_B) | \underline{s}_e(n_B), \theta(e))}{\partial \theta_1} \\ \frac{\partial \pi(\underline{a}_e(1) | \underline{s}_e(1), \theta(e))}{\partial \theta_2} & \dots & \frac{\partial \pi(\underline{a}_e(n_B) | \underline{s}_e(n_B), \theta(e))}{\partial \theta_2} \\ \vdots & \ddots & \vdots \\ \frac{\partial \pi(\underline{a}_e(1) | \underline{s}_e(1), \theta(e))}{\partial \theta_{n_\theta}} & \dots & \frac{\partial \pi(\underline{a}_e(n_B) | \underline{s}_e(n_B), \theta(e))}{\partial \theta_{n_\theta}} \end{bmatrix} \cdot \begin{bmatrix} 1 & \dots & 0 \\ \frac{1}{\pi(\underline{a}_e(1) | \underline{s}_e(1), \theta(e))} & \dots & \vdots \\ \vdots & \ddots & \vdots \\ 0 & \dots & \frac{1}{\pi(\underline{a}_e(n_B) | \underline{s}_e(n_B), \theta(e))} \end{bmatrix}, \quad (9)$$

where the matrix on the left is a transposed Jacobian, i.e., $\dot{\underline{\Pi}}(\underline{s}_e, \underline{a}_e, \theta(e)) = \left(\frac{\partial}{\partial \theta} \underline{\pi}(\underline{a}_e | \underline{s}_e, \theta(e)) \right)^T$. Denote the inverse policies $\frac{1}{\underline{\pi}(\underline{a}_e(k) | \underline{s}_e(k), \theta(e))}$ with $\pi_e^I(k)$ and $\underline{\pi}_e^I(\underline{s}_e, \underline{a}_e, \theta(e)) = \{\pi_e^I(k)\}_{k=1}^{n_B} \in \mathbb{R}^{n_B}$. The change of the agent weights based on batch e is

$$\frac{d\theta(e)}{de} = \dot{\underline{\Pi}}(\underline{s}_e, \underline{a}_e, \theta(e)) \underline{\Gamma}_e(r_e) \underline{\pi}_e^I(\underline{s}_e, \underline{a}_e, \theta(e)) \quad (10)$$

with $\underline{\Gamma}_e(r_e) = \text{diag}(G_e(r_e)) \in \mathbb{R}^{n_B \times n_B}$. Next, write the learning dynamics of the policy, using the chain rule:

$$\frac{\partial \underline{\pi}(\underline{a}_e | \underline{s}_e, \theta(e))}{\partial e} = \frac{\partial}{\partial \theta} \underline{\pi}(\underline{a}_e | \underline{s}_e, \theta(e)) \frac{d\theta(e)}{de}. \quad (11)$$

First, extract $\frac{d\theta(e)}{de}$ as in Eq. (10):

$$\begin{aligned} \frac{\partial \underline{\pi}(\underline{a}_e | \underline{s}_e, \theta(e))}{\partial e} &= \\ \dot{\underline{\Pi}}(\underline{s}_e, \underline{a}_e, \theta(e))^T \dot{\underline{\Pi}}(\underline{s}_e, \underline{a}_e, \theta(e)) \underline{\Gamma}_e(r_e) \underline{\pi}_e^I(\underline{s}_e, \underline{a}_e, \theta(e)). \end{aligned} \quad (12)$$

Note that $\dot{\underline{\Pi}}(\underline{s}_e, \underline{a}_e, \theta(e))^T \dot{\underline{\Pi}}(\underline{s}_e, \underline{a}_e, \theta(e)) = \frac{\partial}{\partial \theta} \underline{\pi}(\underline{a}_e | \underline{s}_e, \theta(e)) \left(\frac{\partial}{\partial \theta} \underline{\pi}(\underline{a}_e | \underline{s}_e, \theta(e)) \right)^T$ is the Neural Tangent Kernel (NTK), as defined in Jacot et al. (2018). Denote it with $\underline{\Theta}_{\underline{\pi}, e}(s, s') \in \mathbb{R}^{n_B \times n_B}$. Finally, the policy update due to episode batch e at states $\underline{s}_e(k)$ for actions $\underline{a}_e(k)$ become:

$$\frac{\partial \underline{\pi}(\underline{a}_e | \underline{s}_e, \theta(e))}{\partial e} = \underline{\Theta}_{\underline{\pi}, e}(s, s') \underline{\Gamma}_e \underline{\pi}_e^I(\underline{s}_e, \underline{a}_e, \theta(e)). \quad (13)$$

Similarly, by defining $\underline{\Pi}_e^I(\underline{s}_e, \underline{a}_e, \theta(e)) = \text{diag}(\underline{\pi}_e^I(\underline{s}_e, \underline{a}_e, \theta(e)))$ we can write Eq. (14) as

$$\frac{\partial \underline{\pi}(\underline{a}_e | \underline{s}_e, \theta(e))}{\partial e} = \underline{\Theta}_{\underline{\pi}, e}(s, s') \underline{\Pi}_e^I(\underline{s}_e, \underline{a}_e, \theta(e)) G_e(r_e) \quad (14)$$

too. \square

Remark 1 From Eq. (13), the learning dynamics of the REINFORCE algorithm is a nonlinear differential equation system. If the same data batch is shown to the neural network over and over again, the policy evolves as $\dot{x}(\tau) = \beta \frac{1}{x(\tau)}$.

2.2 Evaluating the policy change for arbitrary states and actions

In this section, we describe the policy change for any state and any action if the agent learns from batch e . In most cases, the learning agent can perform multiple actions. Assume the agent can take a^1, a^2, \dots, a^{n_A} actions (the policy net has n_A output channels). Previous works that deal with NTK all consider one output channel in the examples (e.g., Bradbury et al. (2018); Jacot et al. (2018); Yang and Salinan (2019)), however state that it works for multiple outputs too. Jacot et al. (2018) claim that a network with n_A outputs can be handled as n_A independent neural networks. On the other hand, it is possible to fit every output channel into one equation by generalizing Theorem 2. First, reconstruct the return vector \underline{G}_e as follows.

$$\underline{G}_e(\underline{a}_e, r_e) = [G_e^{a^1}(1), G_e^{a^2}(1), \dots, G_e^{a^{n_A}}(n_B)]^T \in \mathbb{R}^{n_A n_B}, \quad (15)$$

where

$$G_e^{a^i}(k) = \begin{cases} G_e(k) & \text{if } a^i \text{ is taken at step } k \\ 0 & \text{otherwise} \end{cases} \quad (16)$$

and $i = 1, 2, \dots, n_A$. In other words, $\underline{G}_e(\underline{a}_e, \underline{r}_e)$ consists of $n_A \times 1$ sized blocks with zeros, at action indexes which are not taken at $\underline{s}_e(k)$, ($n_A - 1$ zeros) and the original return (Eq. (4)) at the position of the taken action. Note that action dependency of $\underline{G}_e(\underline{a}_e, \underline{r}_e)$ stems from this assumption.

Theorem 3 *Given batch $\{\underline{s}_e(k), \underline{a}_e(k), \underline{r}_e(k)\}_{k=1}^{n_B}$, and assuming gradient flow, the episodic policy change with the REINFORCE algorithm at the batch states for an n_A output policy network is*

$$\frac{\partial \underline{\pi}(\underline{a} | \underline{s}_e, \theta(e))}{\partial \underline{e}} = \underline{\Theta}_{\pi, e}(s, s') \underline{\Pi}_e^I(\underline{s}_e, \theta(e)) \underline{G}_e(\underline{a}_e, \underline{r}_e),$$

where $\frac{\partial \underline{\pi}(\underline{a} | \underline{s}_e, \theta(e))}{\partial \underline{e}} \in \mathbb{R}^{n_A n_B}$ and $\underline{\Theta}_{\pi, e}(s, s') \in \mathbb{R}^{n_A n_B \times n_A n_B}$.

Proof We can deduce the multi-output case by rewriting Eq. (6). For simplicity, we keep the notations, but the matrix and vector sizes are redefined for the vector output case. Therefore, the log policy derivatives are evaluated for every possible action at the states contained in a batch:

$$\underline{\dot{\Pi}}_{log}(\underline{s}_e, \theta(e)) = \begin{bmatrix} \frac{\partial \log \pi(a^1 | \underline{s}_e(1), \theta(e))}{\partial \theta_1} & \dots & \frac{\partial \pi(a^{n_A} | \underline{s}_e(n_B), \theta(e))}{\partial \theta_1} \log \\ \frac{\partial}{\partial \theta_2} \log \pi(a^1 | \underline{s}_e(1), \theta(e)) & \dots & \frac{\partial \log \pi(a^{n_A} | \underline{s}_e(n_B), \theta(e))}{\partial \theta_2} \\ \vdots & \ddots & \vdots \\ \frac{\partial \log \pi(a^1 | \underline{s}_e(1), \theta(e))}{\partial \theta_{n_\theta}} & \dots & \frac{\partial \log \pi(a^{n_A} | \underline{s}_e(n_B), \theta(e))}{\partial \theta_{n_\theta}} \end{bmatrix}, \quad (17)$$

$\underline{\dot{\Pi}}_{log}(\underline{s}_e, \theta(e)) \in \mathbb{R}^{n_\theta \times n_A n_B}$. The zero elements in $\underline{G}_e(\underline{a}_e, \underline{r}_e)$ will cancel out log probabilities of actions that are not taken in episode e , see Eq. (16). Therefore, the final output $\frac{\partial \underline{\pi}(\underline{a}_e | \underline{s}_e, \theta(e))}{\partial \underline{e}}$ does not change. Note that, the action dependency is moved from $\underline{\dot{\Pi}}_{log}(\underline{s}_e, \theta(e))$ to $\underline{G}_e(\underline{a}_e, \underline{r}_e)$. That is, because the policy is evaluated for every output channel of the policy network, but nonzero reward is given only if an action is actually taken in the MC trajectory. Continue by separating $\underline{\dot{\Pi}}_{log}(\underline{s}_e, \theta(e))$ into two matrices, in the same way as in Eq. (9).

$$\underline{\dot{\Pi}}_{log}(\underline{s}_e, \theta(e)) = \underline{\dot{\Pi}}(\underline{s}_e, \theta(e)) \underline{\Pi}_e^I(\underline{s}_e, \theta(e)) = \begin{bmatrix} \frac{\partial \pi(a^1 | \underline{s}_e(1), \theta(e))}{\partial \theta_1} \frac{\partial \pi(a^2 | \underline{s}_e(1), \theta(e))}{\partial \theta_1} \dots \frac{\partial \pi(a^{n_A} | \underline{s}_e(n_B), \theta(e))}{\partial \theta_1} \\ \frac{\partial \pi(a^1 | \underline{s}_e(1), \theta(e))}{\partial \theta_2} \frac{\partial \pi(a^2 | \underline{s}_e(1), \theta(e))}{\partial \theta_2} \dots \frac{\partial \pi(a^{n_A} | \underline{s}_e(n_B), \theta(e))}{\partial \theta_2} \\ \vdots \\ \frac{\partial \pi(a^1 | \underline{s}_e(1), \theta(e))}{\partial \theta_{n_\theta}} \frac{\partial \pi(a^2 | \underline{s}_e(1), \theta(e))}{\partial \theta_{n_\theta}} \dots \frac{\partial \pi(a^{n_A} | \underline{s}_e(n_B), \theta(e))}{\partial \theta_{n_\theta}} \end{bmatrix}.$$

$$\begin{bmatrix} \frac{1}{\pi(a^1 | \underline{s}_e(1), \theta(e))} & & & \\ & \frac{1}{\pi(a^2 | \underline{s}_e(1)\theta(e))} & & \\ & & \ddots & \\ & & & \frac{1}{\pi(a^{n_A} | \underline{s}_e(n_B), \theta(e))} \end{bmatrix}, \quad (18)$$

where the diagonalized inverse policies are denoted with $\underline{\Pi}_e^I(\underline{s}_e, \theta(e))$. The weight change can be written as

$$\frac{d\theta(e)}{de} = \underline{\dot{\Pi}}(\underline{s}_e, \theta(e)) \underline{\Pi}_e^I(\underline{s}_e, \theta(e)) \underline{G}_e(\underline{a}_e, r_e). \quad (19)$$

Following the same steps as for the proof of Theorem 2, the policy change for every output channel is

$$\frac{\partial \pi(a | \underline{s}_e, \theta(e))}{\partial e} = \underline{\Theta}_{\pi, e}(s, s') \underline{\Pi}_e^I(\underline{s}_e, \theta(e)) \underline{G}_e(\underline{a}_e, r_e). \quad (20)$$

□

Remark 2 It is possible to write the average change of each policy output channel over a batch (with superscript B) as

$$\begin{aligned} \frac{\partial \pi^B(a | \underline{s}_e, \theta(e))}{\partial e} &= \\ \frac{1}{n_B} \underline{E} \underline{\Theta}_{\pi, e}(s, s') \underline{\Pi}_e^I(\underline{s}_e, \theta(e)) \underline{G}_e(\underline{a}_e, r_e). \end{aligned} \quad (21)$$

where \underline{E} is an $n_A \times n_A n_B$ matrix consisting of n_B eye matrices of size $n_A \times n_A$. \underline{E} is used to sum elements that correspond to the same output channel. The result of Eq. (21) is the policy change at an averaged state of \underline{s}_e .

With Theorem 3, it is possible to evaluate how the policy will change at states \underline{s}_e when learning on batch data e if the learning rate is small. By manipulating Eq. (20) policy change can be evaluated at states not part of batch \underline{s}_e too.

Theorem 4 Given batch $\{\underline{s}_e(k), \underline{a}_e(k), r_e(k)\}_{k=1}^{n_B}$, and assuming gradient flow, the episodic policy change with the REINFORCE algorithm at any state $s_0 \notin \underline{s}_e$ is

$$\frac{\partial \pi(a | s_0, \theta(e))}{\partial e} = \underline{\vartheta}(\underline{s}_e, s_0) \underline{\Pi}_e^I(\underline{s}_e, \theta(e)) \underline{G}_e(\underline{a}_e, r_e) \in \mathbb{R}^{n_A},$$

where $\underline{\vartheta}(\underline{s}_e, s_0) = [\underline{\vartheta}(s_1, s_0), \underline{\vartheta}(s_2, s_0), \dots, \underline{\vartheta}(s_{n_B}, s_0)] \in \mathbb{R}^{n_A \times n_A n_B}$ is the neural tangent kernel evaluated for all \underline{s}_e, s_0 pairs.

Proof First, we concatenate the states and returns (\underline{s}_e, s_0) , $(\underline{G}_e(\underline{a}_e, r_e), \underline{G}_0(a_0, r_0))$, respectively and solve Eq. (20) for s_0 . For more insight, we illustrate the matrix multiplication in Eq. (20) with the concatenated state in Figure 1.

$$\begin{aligned} \frac{\partial \pi(a | s_0, \theta(e))}{\partial e} &= \underline{\vartheta}(\underline{s}_e, s_0) \underline{\Pi}_e^I(\underline{s}_e, \theta(e)) \underline{G}_e(\underline{a}_e, r_e) + \\ &+ \underline{\vartheta}(s_0, s_0) \underline{\Pi}_e^I(s_0, \theta(e)) \underline{G}_0(\underline{a}_0, r_0). \end{aligned} \quad (22)$$

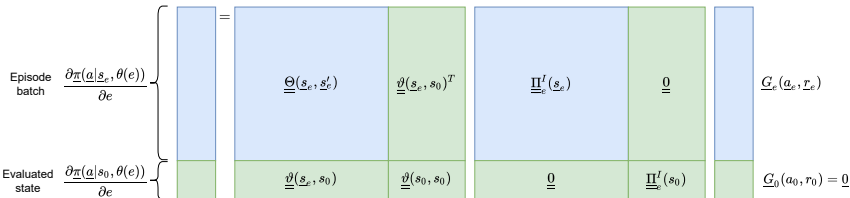


Fig. 1: Matrix compatibility with the augmented batch. The blue section indicates the original Eq. (20), while the green blocks stem from the augmentation.

The NTK is based on the partial derivatives of the policy network and can be evaluated anywhere. Therefore, $\underline{\vartheta}(\underline{s}_e, s_0) = [\underline{\vartheta}(s_1, s_0), \underline{\vartheta}(s_2, s_0), \dots, \underline{\vartheta}(s_{n_B}, s_0)] \in \mathbb{R}^{n_A \times n_A n_B}$ can be computed for any state. $\underline{\vartheta}(\underline{s}_e, s_0)$ consists of symmetric $n_A \times n_A$ blocks. Since s_0 is not included in the learning, it does not affect the policy change, its return is zero for every action, $\underline{G}_0(\underline{a}_0, r_0) = \underline{0} \in \mathbb{R}^{n_A}$. The zero return cancels out the term $\underline{\vartheta}(s_0, s_0) \underline{\Pi}'(s_0, \theta(e)) \underline{G}_0(\underline{a}_0, r_0) \in \mathbb{R}^{n_A}$. Therefore,

$$\frac{\partial \pi(\underline{a} | s_0, \theta(e))}{\partial e} = \underline{\vartheta}(\underline{s}_e, s_0) \underline{\Pi}'(\underline{s}_e, \theta(e)) \underline{G}_e(\underline{a}_e, \underline{r}_e) \in \mathbb{R}^{n_A}. \quad (23)$$

□

3 The NTK-based constrained REINFORCE algorithm

Every physical system has some limits (saturation). Intuitively, the agent should not increase the control action towards the limit if the system is already in saturation (for example, if a robot manipulator is at an end position, increasing the force in the direction of that end position is pointless). Assuming we have some idea how the agent should behave (which actions to take) at specific states $\underline{s}_s = [s_{s1}, s_{s2}, \dots, s_{sn_s}]$ or regions $f_s(t)$, equality and inequality constraints can be prescribed for the policy. Define equality and inequality constraints as $\pi_{ref,eq}(\underline{a}_s | \underline{s}_s) = \underline{c}_{eq}$ and $\pi_{ref,ineq}(\underline{a}_s | \underline{s}_s) \geq \underline{c}_{ineq}$, where $[\underline{c}_{eq}, \underline{c}_{ineq}] \in \mathbb{R}^{n_s}$ is a vector constant probabilities. Additionally, suppose that one constrained region in the state space is described with $f_s(t) : \mathbb{R} \rightarrow \mathcal{S}$. Then, in the constrained regions we assume to have a reference policy $\pi_{ref,reg}(\underline{a}_s | f_s(t)) \geq c_{reg}, \forall t \in [t_{min}, t_{max}]$.

In the sequel, relying on Theorem 4, we provide the mathematical deduction on how to enforce constraints during learning.

3.1 Equality constraints

To deal with constraints, we augment Eq. (20) with the constrained state-action pairs. Visually, the policy change at the augmented batch states are shown in Figure 2. Since the desired policy change at the safe states can be given as

$$\Delta \pi(\underline{a}_s | \underline{s}_s, \theta(e)) = \pi_{ref,eq}(\underline{a}_s | \underline{s}_s) - \pi(\underline{a}_s | \underline{s}_s, \theta(e)), \quad (24)$$

$\Delta\pi(\underline{a}_s \mid \underline{s}_s, \theta(e)) \in \mathbb{R}^{n_s}$. The only unknowns are the returns $\underline{G}_s = [G_{s1}, G_{s2}, \dots, G_{sn_s}]$ for the safe actions at the safe states. Note that the upper block of Figure 2 contains differential equations, while the lower block consists of algebraic equations. It is sufficient to solve the algebraic part. With the lower blocks of Figure 2 we can write the linear equation system

$$\begin{aligned} \Delta\pi(\underline{a}_s \mid \underline{s}_s, \theta(e)) - \underline{\vartheta}(\underline{s}_e, \underline{s}_s) \underline{\Pi}_e^I(\underline{s}_e, \theta(e)) \underline{G}_e(\underline{a}_e, r_e) = \\ \underline{\vartheta}(\underline{s}_s, \underline{s}'_s) \underline{\Pi}_e^I(\underline{s}_s, \theta(e)) \underline{G}_s. \end{aligned} \quad (25)$$

This system has a single unique solution as there are n_S unknown returns and n_S equations and it can be solved with e.g., the DGSEV algorithm Haidar et al. (2018).

$$\frac{\partial\pi(\underline{a}, \underline{a}_s \mid \underline{s}_e, \underline{s}_s, \theta(e))}{\partial e} = \underline{\Theta}(\underline{s}_e, \underline{s}_s), (\underline{s}_e, \underline{s}_s) \quad \underline{\Pi}_e^I(\underline{s}_e, \underline{s}_s) \quad \underline{G}(\underline{a}_e, r_e)$$

Episode batch	}	$\frac{\partial\pi(\underline{a} \mid \underline{s}_e, \theta(e))}{\partial e}$	$\underline{\Theta}(\underline{s}_e, \underline{s}'_e)$	$\underline{\vartheta}(\underline{s}_e, \underline{s}_s)^T$	$\underline{\Pi}_e^I(\underline{s}_e)$	$\underline{0}$	$\underline{G}_e(\underline{a}_e, r_e)$
Constraints		$\Delta\pi(\underline{a}_s \mid \underline{s}_s, \theta(e))$	$\underline{\vartheta}(\underline{s}_e, \underline{s}_s)$	$\underline{\vartheta}(\underline{s}_s, \underline{s}'_s)$	$\underline{0}$	$\underline{\Pi}_e^I(\underline{s}_s)$	\underline{G}_s

Fig. 2: Matrix compatibility of the constrained policy change evaluation (concatenated batch)

In order to obey the constraints, a safe data batch is constructed. We concatenate the safe states, actions, and computed returns with the episode batch as: $\{(\underline{s}_e, \underline{s}_s), (\underline{a}_e, \underline{a}_s), (\underline{G}_e(\underline{a}_e, r_e), \underline{G}_s)\}$. Then, the agent's weights are updated with the appended batch with gradient ascent, Eq. (3).

In the initial stages of learning, the difference between the reference policies and the actual ones will be large. Therefore high rewards are needed to eliminate this difference. This also means that the effect of the collected batch on the weights is minor compared to the safe state-action-return tuples. In addition, large returns might cause loss of stability during the learning. The returns computed from the linearized policy change might differ from the actual one, especially if large steps are taken (i.e., large returns are applied). On the other hand, when the policy obeys the constraints, the computed returns will be small and will only compensate for the effect of the actual batch. In a special case when the return is zero, the result is the unconstrained policy change at the specific state as in Section 2.2. In addition, if the policy is smooth, the action probabilities near the constrained points will be similar. In continuous state space, this implies that defining grid-based (finite) constraints is sufficient.

Remark 3 Time complexity: The critical operations are kernel evaluations and solving the linear equation system. The DGSEV algorithm used for solving the linear equation system has time complexity $\mathcal{O}(n_S^3)$ Haidar et al. (2018). The time complexity of kernel evaluations is $\mathcal{O}((n_B + n_S)n_S)$. If the kernel is computed for every output channel at the batch states, time complexity increases to $\mathcal{O}((n_A n_B + n_S)n_S)$.

3.2 Inequality constraints

In the same way, inequality constraints can be prescribed too. Assume there are some states of the environment where an action shall be taken with at least a constant probability: $\pi_{ref,ineq}(a_s | \underline{s}_s) \geq \underline{c}_{ineq}$. Then, similar to Eq. (25), the inequality constraints can be written as

$$\begin{aligned} \Delta \pi(a_s | \underline{s}_s, \theta(e)) - \underline{\vartheta}(\underline{s}_e, \underline{s}_s) \underline{\Pi}_e^I(\underline{s}_e, \theta(e)) \underline{G}_e(a_e, r_e) \\ \leq \underline{\vartheta}(\underline{s}_s, \underline{s}'_s) \underline{\Pi}_e^I(\underline{s}_s, \theta(e)) \underline{G}_s. \end{aligned} \quad (26)$$

Solving this system of inequalities can be turned into a convex quadratic programming problem. Since the original goal of reinforcement learning is learning on the collected episode batch data, the influence of the constraints on the learning (i.e., the magnitude of \underline{G}_s) should be as small as possible. Therefore, the quadratic program is

$$\min_{G_{si}} \sum_{i=1}^{n_S} G_{si}^2 \quad (27)$$

subject to Eq. (26).

Note that, the quadratic cost function is needed to similarly penalize positive and negative returns. Quadratic programming with interior point methods has polynomial time complexity ($\mathcal{O}(n_S^3)$, Ye and Tse (1989)) and has to be solved after every episode. Alternatively, it is possible to relax the constraints via introducing slack variables Boyd and Vandenberghe (2004). This approach turns the optimization with hard constraints into soft ones, which can be solved even if there are conflicting constraints. In practical applications, such numerical errors are more of an issue than time complexity (i.e. solving the optimization with thousands of constraints).

3.3 Constrained regions - dynamically changing constraints

The equality and inequality constraints we proposed in the previous subsections have some limitations, especially in high-dimensional state spaces. This subsection, explores whether the proposed methodology can be extended to constrained regions of the state space. Note that handling entire regions is computationally very intensive; therefore, we focus our efforts on dynamically changing (within a region) point-wise constraints. Prescribing point-wise constraints is not only computationally easier but also less stringent than constraining whole regions. The prerequisite for satisfying a constraint in a

whole region require powerful function approximators, i.e., neural networks with many tuneable parameters.

In order to handle regional constraints we modify Eq. (26) to admit $f_s(t)$:

$$\begin{aligned} \Delta\pi(a_s | f(t), \theta(e)) - \underline{\vartheta}(\underline{s}_e, f_s(t)) \underline{\Pi}_e^I(\underline{s}_e, \theta(e)) \underline{G}_e(\underline{a}_e, \underline{r}_e) \\ \leq \underline{\vartheta}(f_s(t), f_s(t')) \underline{\Pi}_e^I(f_s(t), \theta(e)) G_s(t). \end{aligned} \quad (28)$$

Note that $G_s(t)$ is a scalar function in this case. I.e., we seek for a return function that forces the policy to obey the prescribed constraint in the region characterized by $f_s(t)$. This yields a non-convex optimization to find $G_s(t)$ that satisfies Eq. (28) $\forall t$.

Under some assumptions, this optimization can be simplified. Assuming $\underline{\vartheta}(f_s(t), f_s(t')) \underline{\Pi}_e^I(f_s(t), \theta(e))$ is positive and invertible $\forall t$, one can write

$$\begin{aligned} \left(\Delta\pi(a_s | f_s(t), \theta(e)) - \underline{\vartheta}(\underline{s}_e, f_s(t)) \underline{\Pi}_e^I(\underline{s}_e, \theta(e)) \underline{G}_e(\underline{a}_e, \underline{r}_e) \right) \\ \left(\underline{\vartheta}(f_s(t), f_s(t')) \underline{\Pi}_e^I(f_s(t), \theta(e)) \right)^{-1} \leq G_s(t). \end{aligned} \quad (29)$$

In other words, $G_s(t)$ is lower-bounded by a nonlinear function. Since we are looking for a single return value instead of a function we pick a single $G_{s_o} \geq G_s(t_o)$, $t_o \in [t_{min}, t_{max}]$. Here we present two approaches to do so.

3.3.1 Maximum return

First, we select t_o where $G_s(t_o)$ has its maximum within $[t_{min}, t_{max}]$. For a continuous t , it can be done by computing the derivative of the left-hand side of Eq. (29):

$$\begin{aligned} \frac{d}{dx} \left[\left(\Delta\pi(a_s | f_s(t), \theta(e)) - \underline{\vartheta}(\underline{s}_e, f_s(t)) \underline{\Pi}_e^I(\underline{s}_e, \theta(e)) \underline{G}_e(\underline{a}_e, \underline{r}_e) \right) \right. \\ \left. \left(\underline{\vartheta}(f_s(t), f_s(t')) \underline{\Pi}_e^I(f_s(t), \theta(e)) \right)^{-1} \right] = 0, \end{aligned} \quad (30)$$

and evaluating the original function at the roots of the above equation and evaluating the original function at these points plus at t_{min} and t_{max} . Then we can select $G_s(t_o)$ that is greater or equal to the local extremum.

The numerical solution to the above is much easier. First, we discretize t with $t_i \in [t_{min}, t_{max}]$ and evaluate Eq. (29) at every t_i .

$$\begin{aligned} t_o = \underset{t_i}{argmax} \left(\left(\Delta\pi(a_s | f_s(t), \theta(e)) - \underline{\vartheta}(\underline{s}_e, f_s(t_i)) \underline{\Pi}_e^I(\underline{s}_e, \theta(e)) \underline{G}_e(\underline{a}_e, \underline{r}_e) \right) \right. \\ \left. \left(\underline{\vartheta}(f_s(t_i), f_s(t_i)) \underline{\Pi}_e^I(f_s(t_i), \theta(e)) \right)^{-1} \right). \end{aligned} \quad (31)$$

Then, we select $G_{s_o} \geq G_s(t_o)$. We use only a single G_{s_o} corresponding to the environment state $f_s(t_o)$ during the episode-by-episode learning. The extremum $G_s(t_o)$ will be at different t values. Therefore, if the function approximator is capable, eventually, the constraint will be satisfied on the whole region. Intuitively, it would be possible to use multiple returns per region, to speed up episode-wise learning at the cost of higher computational demand.

The main drawback of this approach is its computational demand. Despite we use only one constraint per region, we have to evaluate Eq. (29) for every t_i , which involves evaluating the kernel too, which has $\mathcal{O}(n_B + 1)$ time complexity ($n_S = 1$). Therefore, with n_t discrete steps of t , we have $\mathcal{O}(n_B + 1)n_t$.

3.3.2 Maximum policy deviation

It is possible to take a simplified approach. Instead of solving Eq. (29) to find the return that has the most effect in the region, we can look for the point, where the policy deviates the most from the reference (worst-case).

$$t_o = \underset{t}{\operatorname{argmax}} (\pi_{ref,reg}(a_s | f_s(t)) - \pi(a_s | f_s(t), \theta(e))), \quad (32)$$

or in the discrete case

$$t_o = \underset{t_i}{\operatorname{argmax}} (\pi_{ref,reg}(a_s | f_s(t_i)) - \pi(a_s | f_s(t_i), \theta(e))). \quad (33)$$

Then, we solve Eq. (26) for the state $f_s(t_o)$.

Since in these two methods we always select one constrained state per region, these states change episode-by-episode, we could label them dynamic constraint selection too. The dynamical regional constraining methods are further discussed in B through numerical simulations.

Remark 4 Multiple constraints per region. The simplest but least efficient way to tackle regional constraints would be to use every discrete t_i within the region resulting in n_t constraints per region. For large state spaces and fine discretizations, solving the optimization might be numerically challenging. The above two approaches can be extended to multiple returns too. We could select multiple states per region that would affect the learning the most. Additionally, we could further discretize each region.

Remark 5 Other policy gradient methods. One extension of REINFORCE is policy gradient with baseline. There, a baseline (typically the value function) is subtracted from the returns to reduce variance. The policy is then updated with these modified returns using the policy gradient theorem Sutton and Barto (2018). Constraints can be adapted to the policy gradient with baseline too. Since the returns at the constrained states are shaped to satisfy specific action probabilities, baselines should not be subtracted from the safe returns. Therefore, in a constrained REINFORCE with baseline, batch returns are offset by the baseline while the safe returns are not.

We summarize the NTK-based constrained REINFORCE algorithm in Algorithm 2.

Algorithm 2 The NTK-based constrained REINFORCE algorithm

- 1: Initialize $e = 1$.
 - 2: Define equality constraints $\underline{\pi}_{ref,eq}(\underline{a}_s | \underline{s}_s) = \underline{c}_{eq}$.
 - 3: Define inequality constraints $\underline{\pi}_{ref,ineq}(\underline{a}_s | \underline{s}_s) \geq \underline{c}_{ineq}$.
 - 4: Define regional constraints $\underline{\pi}_{ref,reg}(\underline{a}_s | \underline{f}_s(t)) \geq \underline{c}_{reg}$.
 - 5: Initialize the policy network with random θ weights.
 - 6: **while** not converged **do**
 - 7: **for** every regional constraint $(f_{s1}(t), f_{s2}(t), \dots)$ **do**
 - 8: Find the dynamically constrained state $f_s(t_o)$ with
 - 9: "Maximum return" (Eq. (31))
 - 10: **or**
 - 11: "Maximum policy deviation" (Eq. (33))
 - 12: Append $f_s(t_o)$ to the set of constrained states.
 - 13: **end for**
 - 14: Generate a Monte-Carlo trajectory $\{\underline{s}_e(k), \underline{a}_e(k), \underline{r}_e(k)\}$,
 $k = 1, 2, \dots, n_B$ with the current policy $\pi(\underline{a}_e(k) | \underline{s}_e(k), \theta(e))$.
 - 15: **for** the whole MC trajectory $(k = 1, 2, \dots, n_B)$ **do**
 - 16: Compute the returns $G_e(k)$ with Eq. (4).
 - 17: **end for**
 - 18: Construct $\underline{\vartheta}(\underline{s}_e, \underline{s}_s)$, $\underline{\vartheta}(\underline{s}_s, \underline{s}'_s)$, $\underline{\Pi}_e^I(\underline{s}_e, \theta(e))$, $\underline{\Pi}_e^I(\underline{s}_s, \theta(e))$.
 - 19: Compute \underline{G}_s with Eq. (25) **and** Eq. (26).
 - 20: Concatenate the MC batch and the constraints:
 $\{(\underline{s}_e, \underline{s}_s), (\underline{a}_e, \underline{a}_s), (\underline{G}_e(\underline{a}_e, \underline{r}_e), \underline{G}_s)\}$.
 - 21: **for** the augmented MC trajectory $(k = 1, 2, \dots, n_B + n_S)$ **do**
 - 22: Update policy parameters with gradient ascent (Eq. (3)).
 - 23: **end for**
 - 24: Increment e .
 - 25: **end while**
-

4 Experimental studies

We investigate the proposed constrained learning algorithm in two OpenAI gym environments with increasing complexity: Cartpole Barto et al. (1983) and Lunar lander (Figure 3), Brockman et al. (2016). The simplicity of the Cartpole environment enables us to perform in depth analysis of the proposed algorithm. The lunar lander demonstrates its efficiency in higher-dimensional environment.

The learning agent is a 2 layer deep fully-connected ReLU network with softmax output nonlinearity and appropriate input-output sizes (i.e., 4 inputs and 2 outputs for Cartpole, and 8 inputs and 6 outputs for Lunar lander). The



Fig. 3: Visualization of the environments. Left: Cartpole, right: Lunar lander.

hidden layer width is 5000 neurons with bias terms. That is to comply with the assumptions in Jacot et al. (2018), i.e., a shallow and wide neural network. On the other hand, the NTK can be computed for more complex NN structures too e.g., Yang and Salman (2019). Note that the primary purpose is not finding the best function approximator, merely demonstrating the efficiency of the constrained learning. To achieve lazy learning, the learning rate is set to $\alpha = 0.0001$. The small learning rate ensures that the approximation of the policy change remains accurate, see A.

4.1 Cartpole

The cart pole problem (also known as the inverted pendulum) is a common benchmark in control theory as it can be easily modeled as a linear time invariant system Skogestad and Postlethwaite (2007). The goal is to balance a pole to remain upright by horizontally moving the cart. The agent in this environment can take two actions: accelerating the cart left (a^0) or right (a^1). The cart pole has four states: the position of the cart (x), its velocity (\dot{x}), the pole angle (φ), and the pole angular velocity ($\dot{\varphi}$). In the reinforcement learning setting, the agent's goal is to balance the pole as long as possible. Reward is given for every discrete step if the pole is in vertical direction, and the episode ends if the pole falls or successfully balancing for 200 steps. The pass criteria for this gym environment is reaching an average reward of 195 for 100 episodes.

Constraints are implemented through intuition. If the pole is tilted too much right, the cart must move right to balance it, and vice versa. Selecting too many states to constrain slow down the computation significantly while defining conflicting constraints can make Eq. (26) unsolvable. Inequality constraints are imposed on the pole angle and its angular velocity at discrete cart positions resulting in 18 constrained states, see Table C2 in C.

With the proper selection of constraints, it is possible to train the agent in 5 steps. Figure 4 shows the learning of the constrained agent. The agent learns the problem within a few episodes but it can be attributed to the simplicity of the problem and the choice of constraints. For this environment the constraints are chosen based on what the agent should do intuitively. Thus, once the constraints are fulfilled the agent will be able to balance the pole. The agent can only learn new policies at states which are not constrained, thus the final

policy will be sub-optimal (if the constraints are sub-optimal). This is a trade-off between more sample efficient and safe learning and optimality. The episode loss is presented in Figure 5. It is initially large because the constraints are not yet fulfilled (elements in \underline{G}_s are large). Figure 6 depicts the section of the learned policy with the constrained states. The resulting policy is very smooth, and the constraints are respected.

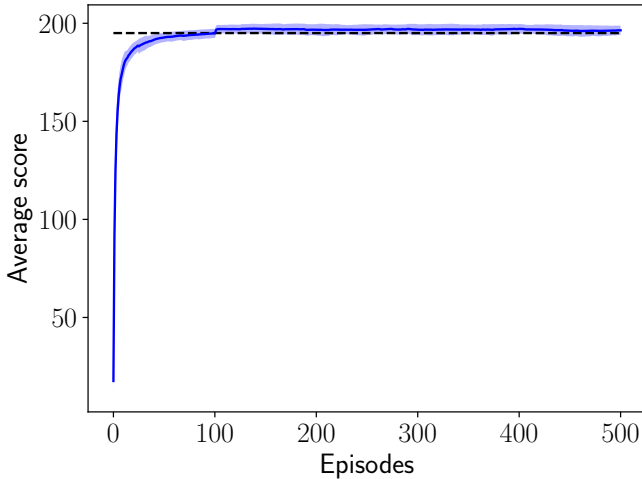
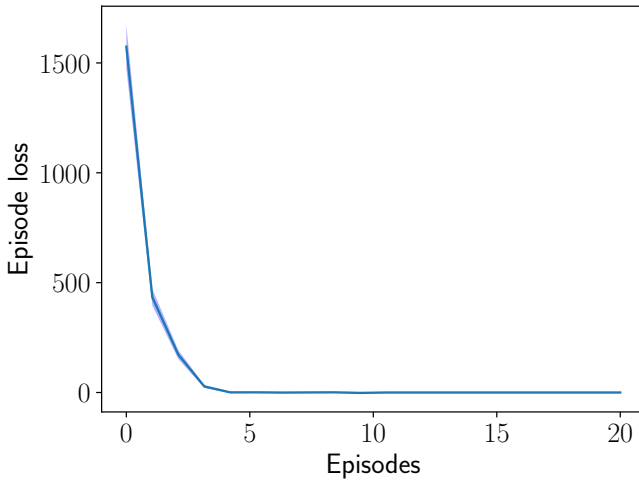
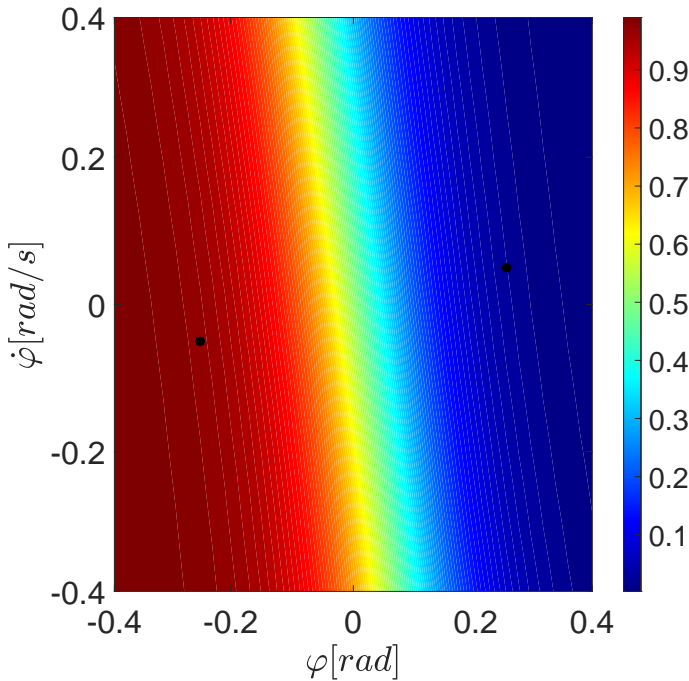


Fig. 4: Solving Cartpole with constrained-PG for 10 different random seeds. Pass criteria is an average score above 195.

**Fig. 5:** Episode loss (Cartpole)**Fig. 6:** Probability of taking a^0 (push the cart left) in the Cartpole environment at $x = 0$, $\dot{x} = 0$. Dots represents the constrained states s_{s5} , s_{s14} (Table C2)

Next, instead of point-wise constraints we introduce constrained regions inspired by Figure 6. We define two main regions bounded by

$$f_1(t) : \dot{\varphi} \leq -8\varphi - 2, \quad (34)$$

$$f_2(t) : \dot{\varphi} \geq -8\varphi + 1.2. \quad (35)$$

Each region is further discretized into three sub-regions (Table C3). Then, each sub-region is discretized into 50 states. We followed the "Maximum policy deviation" constraint selection strategy for every region, yielding 6 dynamically constrained states. Simulation results are on par with the statically constrained simulations, see Figure 7. The agent with the regional constraints learn slightly slower. This is possibly due to the more stringent constraints: there are less constrained states but their location is changing from episode to episode. This is reflected in the evolution of the loss too (Figure 8). It takes more episodes for the loss to disappear and it starts from a higher initial value due to the different selection of constraints. Finally, Figure 9 shows the learned policy, which is almost identical to the statically constrained one.

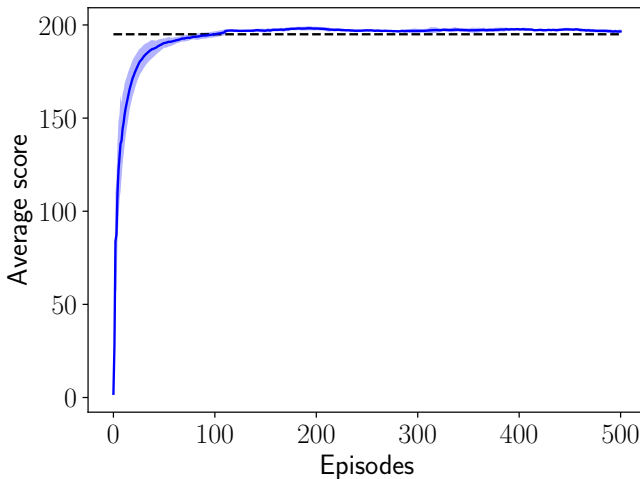


Fig. 7: Solving Cartpole with regionally constrained-PG for 10 different random seeds.

These results would place the algorithm in the top 10 of the OpenAI gym leaderboard for this environment, competing with deterministic policies and closed-loop controllers, and being much faster than traditional RL methods (e.g., Kumar (2020); OpenAI (2021)). Figure 10 shows how the agent learns with the commonly used (unconstrained) double deep Q learning Van Hasselt

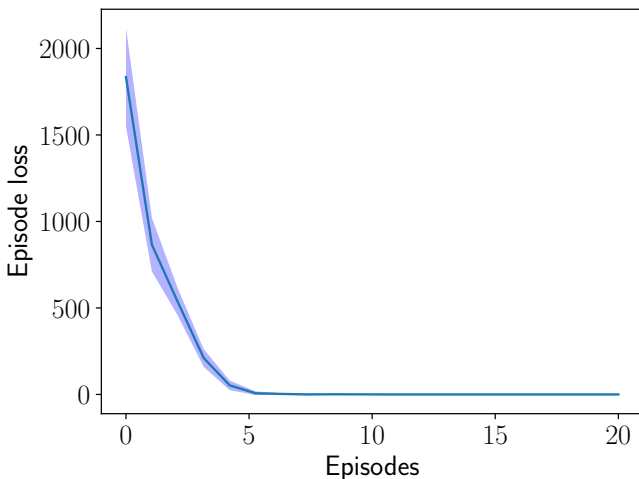


Fig. 8: Episode loss (Cartpole, regional constraints)

et al. (2016). The constraining makes learning much faster as it eliminates the need to explore states that are known to be unsafe.

4.2 Lunar lander

The goal in this 2D environment is to land a rocket on a landing pad without crashing. The agent in this environment has eight states: its horizontal and vertical coordinates (x, y) and velocities (\dot{x}, \dot{y}) , its angle φ , its angular velocity $\dot{\varphi}$ and the logical states whether the left and right legs are in contact with the ground (l_{left} and l_{right}). The agent can choose from four actions: 0: do nothing, 1: fire the left thruster, 2: fire the main engine, and 3: fire the right thruster. The episode finishes if the lander crashes or comes to rest. Reward is given for successfully landing close to the landing pad. Crashing the rocket results in a penalty. Firing the engines (burning fuel) also results in small penalties. In OpenAI gym the pass criteria for solving this environment is an average reward of 200 for 100 episodes.

During unconstrained learning, the two most common reasons observed for episode failures were the lander crashing too fast into the ground and tilting over mid-flight. To this end, constraints were imposed on the vertical velocity and the angle of the lander. Based on these empirical observations we propose inequality constraints.

Constraints are imposed to keep the lander on an ideal trajectory: as the lander comes closer to the ground, it should decelerate by firing the main engine (simulating hover slam). If the rocket has a too large horizontal velocity or is tilted, the side engines should be used. The proposed constraints are summarized in Table C4 (C). In order to ease computational load, only every

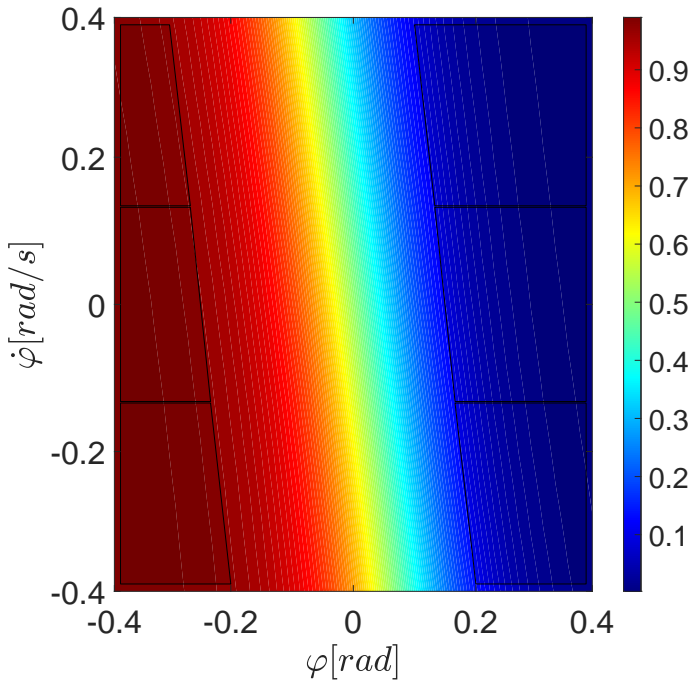


Fig. 9: Probability of taking a^0 (push the cart left) in the Cartpole environment at $x = 0$, $\dot{x} = 0$. Gray regions represent the constraints described in Table C3

10th step of the Monte-Carlo trajectory was logged. Too long trajectories slow down computation as the NTK has to be evaluated at more points, which has polynomial time complexity.

With the above setup, the agent was able to land after a few episodes successfully. However, after 500 episodes of training, the 100 runs average reward was just below 200, see Figure 11. The loss was initially high but since the constraints enforced a "good" policy, it declined quickly.

The results in this environment shed light on some important features of the proposed algorithm. The agent can within a few episodes find a good policy if the constraints are set up right. On the other hand, poor selection of constraints can harm the performance on the long run. The algorithm can achieve similar performance in significantly less steps compared to other benchmarks e.g., Van Hasselt et al. (2016); Gadgil et al. (2020). Figure 12 shows how the agent learns with double deep Q learning Van Hasselt et al. (2016). The unconstrained method learns one order of magnitude slower, however it can reach slightly higher average scores by the end of the training. Therefore, there is a trade-off between speeding up learning via constraining and reaching the

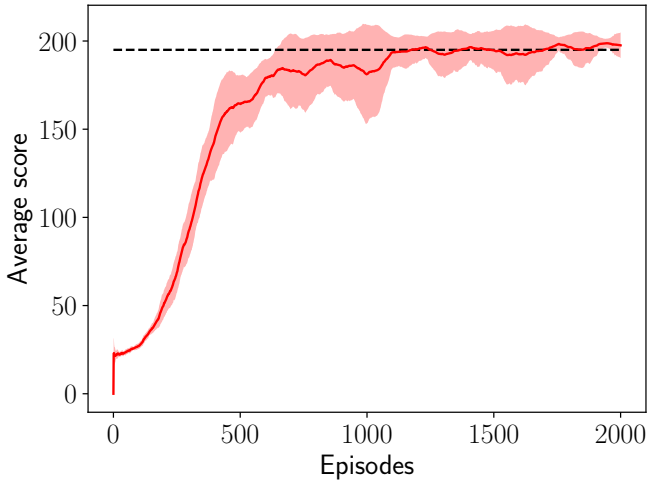


Fig. 10: Solving Cartpole with double deep Q learning for 10 different random seeds.

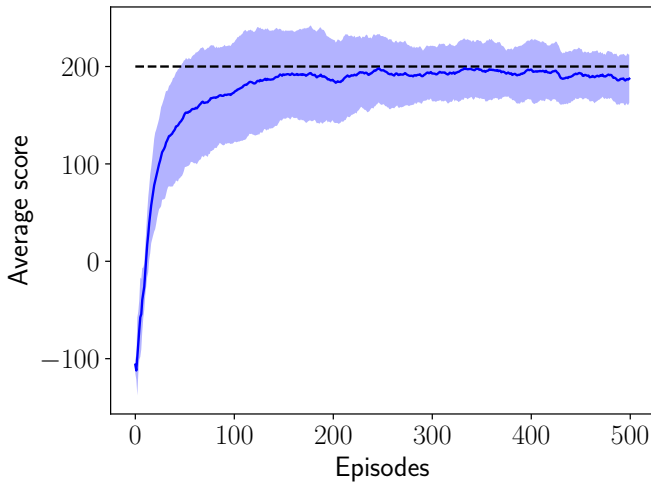


Fig. 11: Solving Lunar lander with constrained-PG for 10 different random seeds. Pass criteria is an average score above 200.

highest possible average score. On the other hand, enforcing constraints during learning reduces oscillations and the variance from different random seeds, that is a common issue for typical benchmarks. Therefore, it is easier to know when to stop learning. With more careful selection of constraint states, the

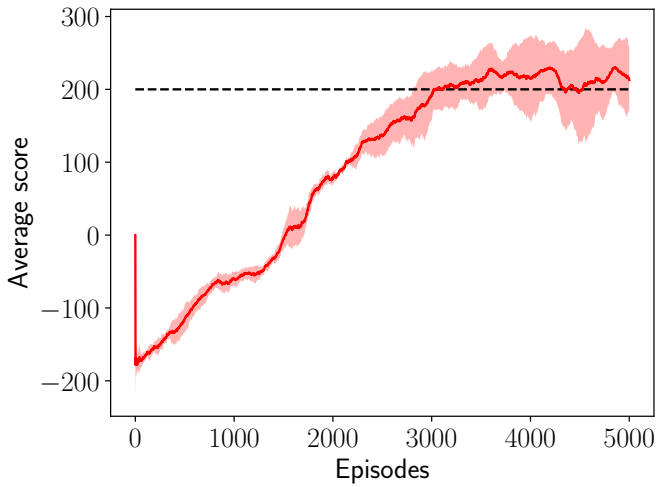


Fig. 12: Solving Lunar lander with double deep Q learning for 10 different random seeds

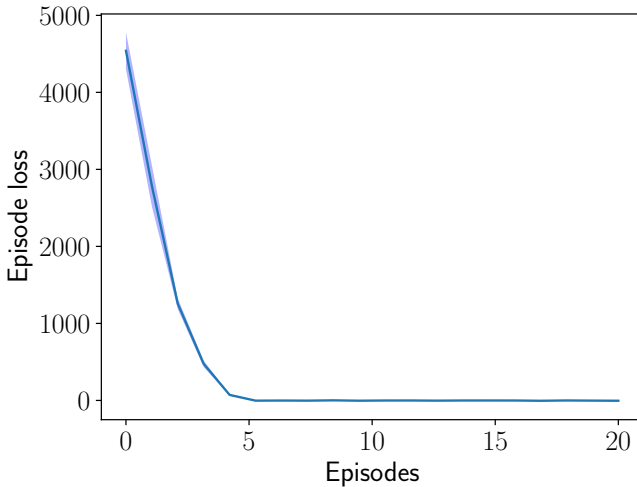


Fig. 13: Episode loss (Lunar lander)

final average score of the agent could be improved, i.e., the constraints would not hamper reaching the optimal policy. This highlights one more drawback of the constrained approach: if the dimension of the environment space is large, the number of required constraints in a grid-based fashion increase significantly

(i.e., the curse of dimensionality applies). Therefore, a lot more manual tuning effort is required to achieve safe and fast learning.

5 Conclusions

We proposed a solution to augment the REINFORCE algorithm with equality, inequality, and dynamically changing regional constraints. To this end, the policy evolution was computed with the help of the neural tangent kernel. Then, arbitrary states were selected with desired action probabilities. Next, for these arbitrary state-action pairs returns were computed that approximately satisfy the prescribed constraints under gradient ascent. The efficiency of the constrained learning was demonstrated with a shallow and wide ReLU network in the Cartpole and Lunar Lander OpenAI gym environments. Results suggest that constraints are satisfied after 2-3 episodes. If they are set up correctly, learning becomes extremely fast (episode-wise) while satisfying safety constraints, thus ensuring some transparency of the policy too. If the constraints are satisfied the returns for safety become small, only slightly influencing learning from the Monte-Carlo trajectory episode batch. On the other hand, selecting suitable constraints requires expert knowledge about the environment. Therefore, the proposed algorithm is best suited for controlled physical systems where saturations and unsafe states can be pinpointed, and countermeasures can be explicitly defined. On the other hand, the learning algorithm may suffer from the curse of dimensionality: in high-dimensional state-spaces setting up constraints manually is tedious. In addition, solving the optimization for several constraints has polynomial time complexity.

As a future line of research, other variants of policy gradient methods will be analyzed. We hypothesize that more complex policy-based approaches can be augmented with constraints using the NTK too. Furthermore, we intend to improve our take on constrained regions. We intend to solve the constrained optimization on a different domain. I.e., transform regional constraints to a domain where they simplify to linear constraints. Note that the proposed "Maximum policy deviation" approach does exactly this in a simplified manner. The transformation is simply the *max* function.

Declarations and statements

Funding

This work has been supported and funded by the project RITE (funded by CHAIR, Chalmers University of Technology).

Statement of interest

The authors have no relevant financial or non-financial interests to disclose.

Ethics approval

Not applicable.

Consent

All authors consent to participating in the paper and publishing their individual data or image.

Author contribution

All authors contributed to the study conception and design. Material preparation, implementation and analysis were performed by Balázs Varga. The first draft of the manuscript was written by Balázs Varga and all authors commented on previous versions of the manuscript. All authors read and approved the final manuscript.

Data availability

Not applicable.

Code availability

Source codes will be made publicly available.

Appendix A Accuracy of the prediction

Due to the linearization in the NTK (gradient calculation), by neglecting the non-differentiable property of the ReLU activation at the origin, as well as by numerical precision errors the NTK-based policy change prediction might be biased. In this appendix this bias is analyzed by comparing the predicted policy update (for the whole batch, Eq. (21)) $\frac{\partial \pi^B(\underline{a}|\underline{s}_e, \theta(e))}{\partial e}$ with the actual one (at the batch average state) $\bar{q}_e(\underline{s}_e, \underline{a}_e, \theta(e), \theta(e+1)) = \frac{1}{n_B} \sum_{k=1}^{n_B} (\pi(a_e(k) | s_e(k), \theta(e+1)) - \pi(a_e(k) | s_e(k), \theta(e)))$, assuming data batch $\{\underline{s}_e, \underline{a}_e, \underline{r}_e\}$. Assuming no constraints, the agent from Section 4.1 tries to learn to balance the pole in the cart pole environment for 100 episodes. The episode-by-episode relative errors during learning are computed with Eq. (A1). Results are shown in Figure A1 for three different learning rates.

$$\varepsilon = \frac{\frac{\partial \pi^B(\underline{a}|\underline{s}_e, \theta(e))}{\partial e} - \bar{q}_e(\underline{s}_e, \underline{a}_e, \theta(e), \theta(e+1))}{(\bar{q}_e(\underline{s}_e, \underline{a}_e, \theta(e), \theta(e+1)))} \cdot 100. \quad (\text{A1})$$

Results suggest that the prediction becomes more accurate as the learning rate decreases. The learning rate used in the simulations (Section 4, $\alpha = 0.001$) yields approximately 0.05% prediction error.

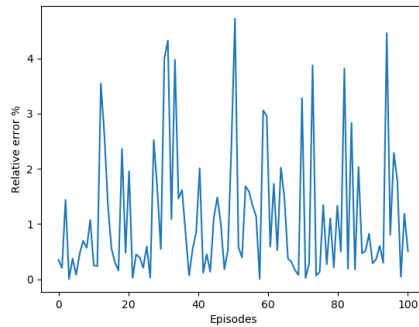
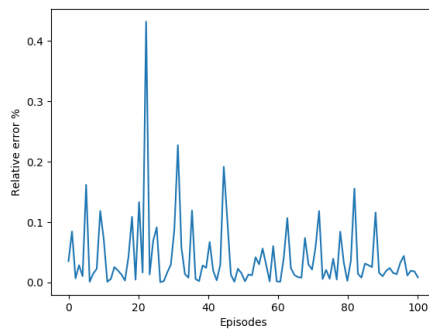
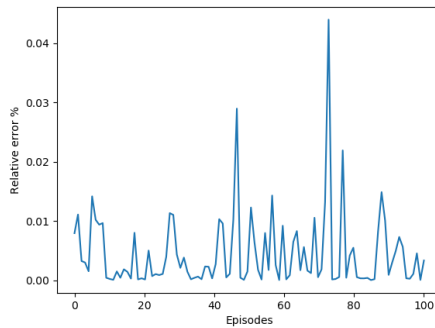
(a) $\alpha = 0.001$ (b) $\alpha = 0.0001$ (c) $\alpha = 0.00001$

Fig. A1: Relative estimation errors between the computed NTK based policy change and the actual, SGD based policy change (Eq. (A1)). Results are shown for the first output channel of the policy network.

Appendix B Simulation-based analysis of the regional constraints

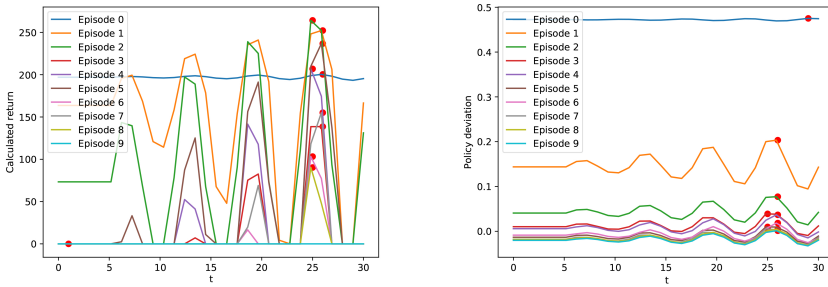
Learning with the regional constraints proposed in Section 3.3 is further investigated using numerical simulations. To this end, the Cartpole environment is used with the agent introduced in Section 4. For visualization purposes, we only consider the last two states of the environment: the pole angle φ , and its angular velocity $\dot{\varphi}$ at the $x = 0, \dot{x} = 0$ slice of the state space. First, we introduce four circular 2D disks as regional constraints, see Table B1. Next, we

	Center	Radius (on φ - $\dot{\varphi}$)	$\pi_{ref,reg}(a^0 f_s(t))$
$f_{s1}(t)$	[0, 0, -0.2 - 0.2]	0.05	≥ 0.95
$f_{s2}(t)$	[0, 0, -0.2 0.2]	0.05	≤ 0.05
$f_{s3}(t)$	[0, 0, 0.2 - 0.2]	0.05	≤ 0.05
$f_{s4}(t)$	[0, 0, 0.2 0.2]	0.05	≥ 0.95

Table B1: Constrained regions

discretize each disk into 30 points (t_i). Then, the constrained learning starts according to the "Maximum return" or the "Maximum policy deviation strategy". In every episode, for every discrete t_o the return is selected with Eq. (31) or Eq. (33), and the environment states corresponding to t_o are used to solve Eq. 26. Selection of t_o with the two strategies is depicted in Figure B2. For both strategies, in the 0^{th} episode, when the policy is initialized randomly (i.e., approximately 50% to take action a^0 everywhere), the computed return or policy deviation is almost the same in the whole region. Then, episode-by-episode, the gain needed or the policy deviation decreases. The location of the state to be constrained is always around the same value. This is due to the presence of the other three regional constraints. For both cases by the 9^{th} episode, the regional constraint is fulfilled (0 computed return, or 0 policy deviation). The sinusoidal nature of $f_{s1}(t)$ stems from the discretization of the disk. Figure B3 summarizes the learning with constrained regions in the state space. In the figure, four episodes are shown with the constrained regions (gray areas) and the corresponding constrained states (stars within the areas). In addition, the trajectory the agent traversed in that episode is shown too (black line). In constrained REINFORCE this trajectory and the constrained states are concatenated. Thus, not only the constrained states but the actual MC trajectory contributes to the learning. However, as long as the constraints are not satisfied the rewards from the MC batch is suppressed by the large returns on the constrained states. Therefore, the two constraint selection strategies yield policies that are only slightly different from each other after learning from 9 episodes.

Note that the prescribed regional constraints in this example are arbitrary and only for demonstration purposes. In the Cartpole environment it yields a bad policy.



(a) Computed returns in region $f_{s1}(t)$ under the "Maximum return" constraining strategy.

(b) Computed policy deviations in region $f_{s1}(t)$ under the "Maximum policy deviation" constraining strategy.

Fig. B2: Functions used in each episode to select the state to constrain

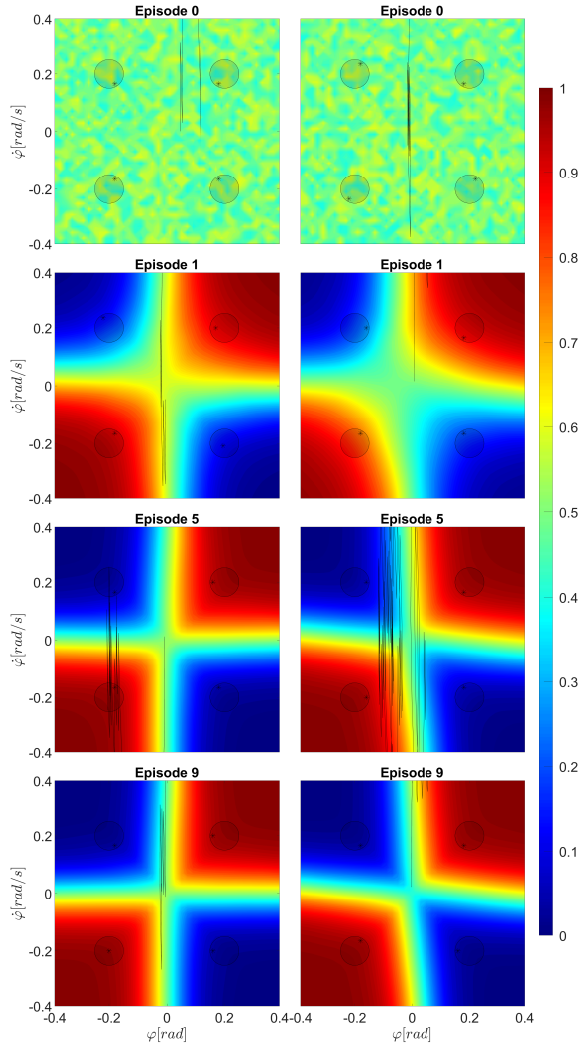


Fig. B3: Probability of taking a^0 in the Cartpole environment at $x = 0$, $\dot{x} = 0$ under regional constraints $f_{s1}(t), \dots, f_{s4}(t)$. Constrained regions are denoted with gray circles, and the actual constrained state $f_s(t_o)$ within each region by a \star . Black lines denote the agent's trajectory in the state-space in the given episode. Plots in the left column show policy evolution with "Maximum return", plots on the right depict the "Maximum policy deviation" constraining strategy.

Appendix C Constraints in the simulations

	x	\dot{x}	φ	$\dot{\varphi}$	$\pi_{ref}(a^0 s_{si})$
s_{s1}	-2	0	0.25	0.05	≤ 0.05
s_{s2}	-1.5	0	0.25	0.05	≤ 0.05
s_{s3}	-1	0	0.25	0.05	≤ 0.05
s_{s4}	-0.5	0	0.25	0.05	≤ 0.05
s_{s5}	0	0	0.25	0.05	≤ 0.05
s_{s6}	0.5	0	0.25	0.05	≤ 0.05
s_{s7}	1	0	0.25	0.05	≤ 0.05
s_{s8}	1.5	0	0.25	0.05	≤ 0.05
s_{s9}	2	0	0.25	0.05	≤ 0.05
s_{s10}	-2	0	-0.25	-0.05	≤ 0.95
s_{s11}	-1.5	0	-0.25	-0.05	≥ 0.95
s_{s12}	-1	0	-0.25	-0.05	≥ 0.95
s_{s13}	-0.5	0	-0.25	-0.05	≥ 0.95
s_{s14}	0	0	-0.25	-0.05	≥ 0.95
s_{s15}	0.5	0	-0.25	-0.05	≥ 0.95
s_{s16}	1	0	-0.25	-0.05	≥ 0.95
s_{s17}	1.5	0	-0.25	-0.05	≥ 0.95
s_{s18}	2	0	-0.25	-0.05	≥ 0.95

Table C2: Constrained states in Cartpole

		$\pi_{ref,reg}(a^0 f_s(t))$
$f_{s1a}(t)$	x bounds: $[-2.5, 2.5]$ \dot{x} bounds: 0 Bounding rectangle on $\varphi\text{-}\dot{\varphi}$: $(-0.4, 0.4)$ $(-0.3, 0.4)$ $(-0.267, 0.133)$ $(-0.4, 0.133)$	≥ 0.95
$f_{s1b}(t)$	x bounds: $[-2.5, 2.5]$ \dot{x} bounds: 0 Bounding rectangle on $\varphi\text{-}\dot{\varphi}$: $(-0.4, 0.133)$ $(-0.267, 0.133)$ $(-0.233, -0.133)$ $(-0.4, -0.133)$	≥ 0.95
$f_{s1c}(t)$	x bounds: $[-2.5, 2.5]$ \dot{x} bounds: 0 Bounding rectangle on $\varphi\text{-}\dot{\varphi}$: $(-0.4, -0.133)$ $(-0.233, -0.133)$ $(-0.2, -0.4)$ $(-0.4, -0.4)$	≥ 0.95
$f_{s2a}(t)$	x bounds: $[-2.5, 2.5]$ \dot{x} bounds: 0 Bounding rectangle on $\varphi\text{-}\dot{\varphi}$: $(0.4, -0.4)$ $(0.2, -0.4)$ $(0.167, -0.133)$ $(0.4, -0.133)$	≤ 0.05
$f_{s2b}(t)$	x bounds: $[-2.5, 2.5]$ \dot{x} bounds: 0 Bounding rectangle on $\varphi\text{-}\dot{\varphi}$: $(0.4, -0.133)$ $(0.167, -0.133)$ $(0.133, 0.133)$ $(0.4, 0.133)$	≤ 0.05
$f_{s2c}(t)$	x bounds: $[-2.5, 2.5]$ \dot{x} bounds: 0 Bounding rectangle on $\varphi\text{-}\dot{\varphi}$: $(0.4, 0.133)$ $(0.133, 0.133)$ $(0.1, 0.4)$ $(0.4, 0.4)$	≤ 0.05

Table C3: Constrained regions in Cartpole

	x	y	\dot{y}	φ	l	$\pi_{ref} \geq 0.95$
s_{s1}	0	0	0	0	1	$j = 0$
s_{s2}	0	0.9	-1	0	0	$j = 2$
s_{s3}	0	0.5	-0.75	0	0	$j = 2$
s_{s4}	0	0.2	-0.5	0	0	$j = 2$
s_{s5}	0	0.1	-0.5	0	0	$j = 2$
s_{s6}	0	1	0	-0.25	0	$j = 1$
s_{s7}	0	1	0	0.25	0	$j = 3$
s_{s8}	0	0.5	0	-0.25	0	$j = 1$
s_{s9}	0	0.5	0	0.25	0	$j = 3$
s_{s10}	0.3	1.3	0.1	0	0	$j = 1$
s_{s11}	-0.3	1.3	-0.1	0	0	$j = 3$

Table C4: Constrained states in Lunar lander

References

- Altman, E. 1999. *Constrained Markov decision processes*, Volume 7. Florida, USA: CRC Press.
- Altman, E., S. Boularouk, and D. Josselin 2019. Constrained markov decision processes with total expected cost criteria. In *Proceedings of the 12th EAI International Conference on Performance Evaluation Methodologies and Tools*, March 13-15, 2019, Palma de Mallorca, Spain, pp. 191–192.
- Arulkumaran, K., M.P. Deisenroth, M. Brundage, and A.A. Bharath. 2017. Deep reinforcement learning: A brief survey. *IEEE Signal Processing Magazine* 34(6): 26–38. <https://doi.org/10.1109/MSP.2017.2743240> .
- Barto, A.G., R.S. Sutton, and C.W. Anderson. 1983. Neuronlike adaptive elements that can solve difficult learning control problems. *IEEE Transactions on Systems, Man, and Cybernetics* 1(5): 834–846. <https://doi.org/10.1109/TSMC.1983.6313077> .
- Berkenkamp, F., M. Turchetta, A. Schoellig, and A. Krause 2017. Safe model-based reinforcement learning with stability guarantees. In *31st Conference on Neural Information Processing Systems (NIPS)*, 4-9 December 2017, Long Beach, CA, US, pp. 908–918.
- Boyd, S. and L. Vandenberghe. 2004. *Convex optimization*. Cambridge, United Kingdom: Cambridge university press.
- Bradbury, J., R. Frostig, P. Hawkins, M.J. Johnson, C. Leary, D. Maclaurin, G. Necula, A. Paszke, J.V. der Plas, S. Wanderman-Milne, and Q. Zhang 2018. *JAX: composable transformations of Python+NumPy programs*.
- Brockman, G., V. Cheung, L. Pettersson, J. Schneider, J. Schulman, J. Tang, and W. Zaremba. 2016. OpenAI Gym. *arXiv preprint arXiv:1606.01540* .
- Cheng, C.A., X. Yan, and B. Boots 2020. Trajectory-wise control variates for variance reduction in policy gradient methods. In *Proceedings of the Conference on Robot Learning*, 16 - 18, November, 2020, Virtually, pp. 1379–1394. PMLR.
- Fisac, J.F., A.K. Akametalu, M.N. Zeilinger, S. Kaynama, J. Gillula, and C.J. Tomlin. 2018. A general safety framework for learning-based control in uncertain robotic systems. *IEEE Transactions on Automatic Control* 64(7): 2737–2752. <https://doi.org/10.1109/TAC.2018.2876389> .
- Gadgil, S., Y. Xin, and C. Xu. 2020. Solving the lunar lander problem under uncertainty using reinforcement learning. *arXiv preprint arXiv:2011.11850* .

- Garcia, J. and F. Fernandez. 2015. A comprehensive survey on safe reinforcement learning. *Journal of Machine Learning Research* 16(42): 1437–1480 .
- Goumri, I.R., B.W. Priest, and M.D. Schneider 2020. Reinforcement learning via gaussian processes with neural network dual kernels. In *2020 IEEE Conference on Games (CoG)*, 24-27 August 2020, Osaka, Japan, pp. 1–8. IEEE.
- Haidar, A., S. Tomov, J. Dongarra, and N.J. Higham 2018. Harnessing gpu tensor cores for fast FP16 arithmetic to speed up mixed-precision iterative refinement solvers. In *SC18: International Conference for High Performance Computing, Networking, Storage and Analysis*, 11-16 November 2018, Dallas, TX, US, pp. 603–613. IEEE.
- Han, F., Q.H. Ling, and D.S. Huang. 2008. Modified constrained learning algorithms incorporating additional functional constraints into neural networks. *Information Sciences* 178(3): 907–919. <https://doi.org/10.1016/j.ins.2007.09.008> .
- Jacot, A., F. Gabriel, and C. Hongler. 2018. Neural tangent kernel: Convergence and generalization in neural networks. *arXiv preprint arXiv:1806.07572* .
- Kakade, S.M. 2001. A natural policy gradient. *Advances in neural information processing systems* 14 .
- Kumar, S. 2020. Balancing a cartpole system with reinforcement learning—a tutorial. *arXiv preprint arXiv:2006.04938* .
- Novak, R., L. Xiao, J. Hron, J. Lee, A.A. Alemi, J. Sohl-Dickstein, and S.S. Schoenholz. 2019. Neural tangents: Fast and easy infinite neural networks in python. *arXiv preprint arXiv:1912.02803* .
- OpenAI. 2021, July. Openai gym leaderboard. <https://github.com/openai/gym/wiki/Leaderboard>.
- Parikh, N. and S. Boyd. 2014. Proximal algorithms. *Foundations and Trends in optimization* 1(3): 127–239. <https://doi.org/10.1561/2400000003> .
- Rasmussen, C.E., M. Kuss, et al. 2003. Gaussian processes in reinforcement learning. In *Advances in neural information processing systems (NIPS)*, Volume 4, pp. 751—758.
- Silver, D., G. Lever, N. Heess, T. Degris, D. Wierstra, and M. Riedmiller 2014. Deterministic policy gradient algorithms. In *Proceedings of the 31st International Conference on Machine Learning*, Volume 32, 21-26 June 2014,

- Beijing, China, pp. 387–395. PMLR.
- Skogestad, S. and I. Postlethwaite. 2007. *Multivariable feedback control: analysis and design*, Volume 2. New York: Wiley.
- Sohl-Dickstein, J., R. Novak, S.S. Schoenholz, and J. Lee. 2020. On the infinite width limit of neural networks with a standard parameterization. *arXiv preprint arXiv:2001.07301* .
- Sutton, R.S. and A.G. Barto. 2018. *Reinforcement learning: An introduction*. Cambridge, Massachusetts, United States: MIT press.
- Szepesvári, C. 2010. Algorithms for reinforcement learning. *Synthesis lectures on artificial intelligence and machine learning* 4(1): 1–103 .
- Tessler, C., D.J. Mankowitz, and S. Mannor. 2018. Reward constrained policy optimization. *arXiv preprint arXiv:1805.11074* .
- Turchetta, M., A. Kolobov, S. Shah, A. Krause, and A. Agarwal 2020. Safe reinforcement learning via curriculum induction. In *Advances in Neural Information Processing Systems (NIPS)*, Volume 33, pp. 1–12.
- Uchibe, E. and K. Doya 2007. Constrained reinforcement learning from intrinsic and extrinsic rewards. In *IEEE 6th International Conference on Development and Learning*, 11-13 July 2007, London, UK, pp. 163–168. IEEE.
- Van Hasselt, H., A. Guez, and D. Silver 2016. Deep reinforcement learning with double Q-learning. In *Proceedings of the AAAI conference on artificial intelligence*, Volume 30.
- Wachi, A. and Y. Sui 2020. Safe reinforcement learning in constrained markov decision processes. In *International Conference on Machine Learning*, pp. 9797–9806. PMLR.
- Whiteson, S. 2020. Expected policy gradients for reinforcement learning. *Journal of Machine Learning Research* 21: 1–51 .
- Williams, R. 1987. A class of gradient-estimation algorithms for reinforcement learning in neural networks. In *Proceedings of the International Conference on Neural Networks*, pp. 591–601.
- Yang, G. and H. Salman. 2019. A fine-grained spectral perspective on neural networks. *arXiv preprint arXiv:1907.10599* .
- Yang, T. 2019. Advancing non-convex and constrained learning: Challenges and opportunities. *AI Matters* 5(3): 29–39. <https://doi.org/10.1145/3362077.3362085> .

- Ye, Y. and E. Tse. 1989. An extension of karmarkar’s projective algorithm for convex quadratic programming. *Mathematical programming* 44(1): 157–179. <https://doi.org/10.1007/BF01587086> .
- Zhang, K., Z. Yang, and T. Başar. 2021. Multi-agent reinforcement learning: A selective overview of theories and algorithms. *Handbook of Reinforcement Learning and Control*: 321–384. https://doi.org/10.1007/978-3-030-60990-0_12 .
- Zimmer, C., M. Meister, and D. Nguyen-Tuong 2018. Safe active learning for time-series modeling with gaussian processes. In *Advances in Neural Information Processing Systems (NIPS)*, pp. 2730–2739.